Mistuning identification for industrial blisks based on the best achievable eigenvector

P. Pichot, D. Laxalde, Jean-Jacques Sinou, Fabrice Thouverez, J.-P. Lombard

Journal home page: http://www.sciencedirect.com/science/journal/00457949

Mistuning identification for industrial blisks based on the best achievable eigenvector
Computers & Structures, *Volume 84, Issues 29-30*, *November 2006*, *Pages 2033-2049*
F. Pichot, D. Laxalde, J.-J. Sinou, F. Thouverez and J.-P. Lombard

MISTUNING IDENTIFICATION FOR INDUSTRIAL BLISKS BASED ON THE BEST ACHIEVABLE EIGENVECTOR

F. PICHOT [1] , D. LAXALDE[1 2,] J-J. SINOU [1 *,] F. THOUVEREZ [1] and J-P. LOMBARD [2]

[1] Laboratoire de Tribologie et Dynamique des Systèmes UMR CNRS 5513
36 avenue Guy de Collongue, Ecole Centrale de Lyon,69134 Ecully, France.

[2] Snecma Moteurs, Site de Villaroche, 77550 Moissy-Cramayel, France

ABSTRACT

This paper presents a method of mistuning identification for industrial blisks from measurements of the system modes and natural frequencies. The procedure is based on the "Best Achievable Eigenvectors" of all measured modes simultaneously combined with a regulation technique. Four illustrative numerical simulations, based on a reduced order model of the blisk, are given which demonstrate that this technique produces acceptable mistuning identification. To do so, a finite element model of the bladed disk and a computational reduced-order modelling technique, based on component mode substitution method and combined with a cyclic characteristic of the blade assembly, are developed. Moreover, sensibility coefficients of the mistuning parameter with respect to measured data are derived.

1 INTRODUCTION

Turbomachinery bladed disks are originally designed to be cyclically symmetric but, because of several inherent phenomena such as manufacturing tolerances, material inhomogeneity or in service wear, small differences appear between each of their elementary sectors. This phenomenon is known as mistuning and is an important concern in this industrial community [1-6]. The first consequence of mistuning on the free response is the frequency splitting of double modes for each circumferencial mode. An associated phenomenon is the eigenvalue loci veering when mistuning changes [7]. The most important consequence is the energy localization in some parts of the structure; it can occur in free [8-9] and in forced response [5,10-14]. Concerning forced response, vibration amplitudes can be 2 to 3 times greater than for the tuned case [11], leading to high-cycle fatigue. However one positive aspect of mistuning is that in some cases, margins to flutter are increased by the presence of mistuning [15].

In the design process of bladed disks, taking mistuning into account raises several subjects of investigation. First predictive models need to be developed; the main issue is that we are studying a mistuned bladed disk, the cyclic symmetry assumption is no longer valid and as a consequence, the structure needs to be modeled entirely (in 360°) which is very expensive. To overcome this problem, these approaches have been developed, first based on lumped parameter model [16] and more and more on reduced order model that can be applied to realistic models [17-21]. In these

models, mistuning is commonly introduced as parameters that perturb each blade natural frequency. Then using these models, some determinist is predictions of free and forced response or eventually some stability analysis can be done. For example, if mistuning parameters are known in terms of their mean and standard deviation, statistic methods can be employed to calculate the probability density function of the blade forced response amplitude [13]. Finally in order to properly evaluate these responses, the mistuning parameters need to be identified in order to update models. This can only be done through experimental investigations. Mistuning identification also allows the designer to check whether the mistuning of a given bladed disk lies within the manufacturing tolerances. In bladed disk assemblies, mistuning identification can be achieved through individual tests on each blade, and the mistuning is defined as the deviations of the blade's natural frequencies with respect to their nominal value (*ie* tuned). However, in single-piece structures such blisks (integrally bladed disks) or blings, individual measurements are no longer possible and mistuning identification using measurements of the system modes and natural frequencies is essential [16-18, 22]. In recent years, several methods have been developed to identify mistuning [23-25].

In this paper, an identification technique is presented. Assuming that global measurements are available, an updating procedure of a reduced-order model of an industrial blisk is performed. The measured modes are treated simultaneously using the "Best Achievable Eigenvector" in combination with a regulation technique [26-27].

First, the reduced order modeling technique used in the mistuning identification method will be briefly presented. Then, the identification technique based on the "Best Achievable Eigenvector" is developed. This method is combined with regularization of measured eigenvectors in order to eliminate part of measured modes which are not realizable with mistuned model considered. The method is then validated numerically on an industrial blisk model; various mistuning distributions are introduced in the reduced-order model and the validation consists in the identification of these mistunings. Finally, sensitivity coefficients of mistuning parameter to measured data is investigated, first theoretically and then applied to the considered model.

2 REDUCED ORDER MODELING OF MISTUNED BLADED DISKS

2.1 Reduced order model

As mentioned in the introduction, mistuned bladed disks cannot be studied using the cyclic symmetry assumption; however since the entire finite element of an industrial blisk will be to expensive in terms of computation time, the use of reduced order modeling technique became unavoidable. For many years, various reduced order models have been proposed in the literature. We refer the interested reader to the papers [20-21,28-36] in order to find an extensive overview of the reduced order modeling techniques that are not the subject of this study. The technique presented here is similar to the component mode substitution method of Benfield and Hruda [37], and is adapted to bladed disk modeling. The main advantage is that mistuning can be easily introduced as perturbation of the cantilevered-blade modes. Recently more efficient methods have been developed which require fewer input data [30,32]. We do not pretend to give an important contribution in this section; the only purpose is to give an overview of the various steps that will be useful for the understanding of this paper.

For this component mode technique, the blades and the disk are thought (naturally) as distinct component substructures and an interface is defined between them. The motion of the entire bladed disk is described using two sets of modes: disk modes with loaded interface (for all nodal diameter) and cantilevered-blade modes, each of these modes being calculated using a finite element method.

The blade motion is constructed using a Craig-Bampton technique, that is a truncated set $\boldsymbol{\Psi}$ of modes of vibration with fixed interface and a set $\boldsymbol{\Theta}$ of constraint modes. By applying this technique, displacement for each blade can be written by

$$ {}^{\mathrm{b}}\tilde{\mathbf{u}} = \begin{bmatrix} \tilde{\boldsymbol{\Theta}} & {}^{\mathrm{b}}\tilde{\boldsymbol{\Psi}} \end{bmatrix} \begin{Bmatrix} {}^{\mathrm{b}}\tilde{\mathbf{u}}_{\mathrm{j}} \\ {}^{\mathrm{b}}\tilde{\mathbf{q}} \end{Bmatrix} \tag{1} $$

By applying the cyclicity argument, the displacements of all blades can be obtained

$$ {}^{\mathrm{b}}\mathbf{u} = \begin{bmatrix} \boldsymbol{\Theta} & {}^{\mathrm{b}}\boldsymbol{\Psi} \end{bmatrix} \begin{Bmatrix} {}^{\mathrm{b}}\mathbf{u}_{\mathrm{j}} \\ {}^{\mathrm{b}}\mathbf{q} \end{Bmatrix} \tag{2} $$

Then, the disk is characterized by its modes with loaded interface, for all possible *P* nodal diameter.

$$ {}^{\mathrm{d}}\mathbf{u} = \sum_{k=0}^{P} {}^{\mathrm{d}}\boldsymbol{\Phi}_k \, {}^{\mathrm{d}}\mathbf{q}_k = {}^{\mathrm{d}}\boldsymbol{\Phi} \, {}^{\mathrm{d}}\mathbf{q} \tag{3} $$

Considering the displacement compatibility over the components (i.e. ${}^{\mathrm{b}}\mathbf{u}_{\mathrm{j}} = {}^{\mathrm{d}}\mathbf{u}_{\mathrm{j}}$), one has

$$ {}^{\mathrm{b}}\mathbf{u} = \begin{bmatrix} \boldsymbol{\Theta} \, {}^{\mathrm{d}}\boldsymbol{\Phi}_{\mathrm{j}} & {}^{\mathrm{b}}\boldsymbol{\Psi} \end{bmatrix} \begin{Bmatrix} {}^{\mathrm{d}}\mathbf{q} \\ {}^{\mathrm{b}}\mathbf{q} \end{Bmatrix} \tag{4} $$

Thus, the transformation matrix $\mathbf{T}$ between physical coordinates $\mathbf{u}$ and modal coordinates $\mathbf{q}$ is given by

$$ \mathbf{T} = \begin{bmatrix} {}^{\mathrm{d}}\boldsymbol{\Phi}_0 & \cdots & {}^{\mathrm{d}}\boldsymbol{\Phi}_k & \cdots & {}^{\mathrm{d}}\boldsymbol{\Phi}_P & \mathbf{0} \\ \boldsymbol{\Theta} \, {}^{\mathrm{d}}\boldsymbol{\Phi}_0 & \cdots & \boldsymbol{\Theta} \, {}^{\mathrm{d}}\boldsymbol{\Phi}_{\mathrm{j}k} & \cdots & \boldsymbol{\Theta} \, {}^{\mathrm{d}}\boldsymbol{\Phi}_{\mathrm{j}P} & {}^{\mathrm{b}}\boldsymbol{\Psi} \end{bmatrix} = \begin{bmatrix} {}^{\mathrm{d}}\boldsymbol{\Phi} & \mathbf{0} \\ \boldsymbol{\Theta} \, {}^{\mathrm{d}}\boldsymbol{\Phi}_{\mathrm{j}} & {}^{\mathrm{b}}\boldsymbol{\Psi} \end{bmatrix} \tag{5} $$

Finally, the synthesized mass and stiffness matrices take the following forms

$$ \bar{\mathbf{M}} = \mathbf{T}^{T} \begin{bmatrix} {}^{\mathrm{d}}\mathbf{M} & \mathbf{0} \\ \mathbf{0} & {}^{\mathrm{b}}\mathbf{M} \end{bmatrix} \mathbf{T} = \begin{bmatrix} \bar{\mathbf{M}}_{\mathbf{dd}} & \bar{\mathbf{M}}_{\mathbf{db}} \\ \bar{\mathbf{M}}_{\mathbf{bd}} & \bar{\mathbf{M}}_{\mathbf{bb}} \end{bmatrix} = \begin{bmatrix} {}^{\mathrm{d}}\boldsymbol{\Phi}^{\mathrm{T}} \, {}^{\mathrm{d}}\mathbf{M} \, {}^{\mathrm{d}}\boldsymbol{\Phi} + \left(\boldsymbol{\Theta} \, {}^{\mathrm{d}}\boldsymbol{\Phi}_{\mathrm{j}} \right)^{\mathrm{T}} {}^{\mathrm{b}}\mathbf{M} \boldsymbol{\Theta} \, {}^{\mathrm{d}}\boldsymbol{\Phi}_{\mathrm{j}} & {}^{\mathrm{b}}\boldsymbol{\Psi}^{\mathrm{T}} \, {}^{\mathrm{b}}\mathbf{M} \boldsymbol{\Theta} \, {}^{\mathrm{d}}\boldsymbol{\Phi}_{\mathrm{j}} \\ {}^{\mathrm{b}}\boldsymbol{\Psi}^{\mathrm{T}} \, {}^{\mathrm{b}}\mathbf{M} \boldsymbol{\Theta} \, {}^{\mathrm{d}}\boldsymbol{\Phi}_{\mathrm{j}} & {}^{\mathrm{b}}\boldsymbol{\Psi}^{\mathrm{T}} \, {}^{\mathrm{b}}\mathbf{M} \, {}^{\mathrm{b}}\boldsymbol{\Psi} \end{bmatrix} \tag{6} $$

$$ \bar{\mathbf{K}} = \mathbf{T}^{T} \begin{bmatrix} {}^{\mathrm{d}}\mathbf{K} & \mathbf{0} \\ \mathbf{0} & {}^{\mathrm{b}}\mathbf{K} \end{bmatrix} \mathbf{T} = \begin{bmatrix} \bar{\mathbf{K}}_{\mathbf{dd}} & \bar{\mathbf{K}}_{\mathbf{db}} \\ \bar{\mathbf{K}}_{\mathbf{bd}} & \bar{\mathbf{K}}_{\mathbf{bb}} \end{bmatrix} = \begin{bmatrix} {}^{\mathrm{d}}\boldsymbol{\Phi}^{\mathrm{T}} \, {}^{\mathrm{d}}\mathbf{K} \, {}^{\mathrm{d}}\boldsymbol{\Phi} + \left(\boldsymbol{\Theta} \, {}^{\mathrm{d}}\boldsymbol{\Phi}_{\mathrm{j}} \right)^{\mathrm{T}} {}^{\mathrm{b}}\mathbf{K} \boldsymbol{\Theta} \, {}^{\mathrm{d}}\boldsymbol{\Phi}_{\mathrm{j}} & {}^{\mathrm{b}}\boldsymbol{\Psi}^{\mathrm{T}} \, {}^{\mathrm{b}}\mathbf{K} \boldsymbol{\Theta} \, {}^{\mathrm{d}}\boldsymbol{\Phi}_{\mathrm{j}} \\ {}^{\mathrm{b}}\boldsymbol{\Psi}^{\mathrm{T}} \, {}^{\mathrm{b}}\mathbf{K} \boldsymbol{\Theta} \, {}^{\mathrm{d}}\boldsymbol{\Phi}_{\mathrm{j}} & {}^{\mathrm{b}}\boldsymbol{\Psi}^{\mathrm{T}} \, {}^{\mathrm{b}}\mathbf{K} \, {}^{\mathrm{b}}\boldsymbol{\Psi} \end{bmatrix} \tag{7} $$

2.2 Model of mistuning

Structural mistuning refers to nonuniformities in structural parameters around a bladed disk which are due to inherent causes. Generally speaking, disk mistuning is negligible versus blade mistuning; that's why it is considered as perturbation of the structural parameters of the blades. Moreover, there exist several type of mistuning which are frequency, damping or form mistuning; but it is commonly assumed that only frequency and in some cases damping mistuning are considered [28]. As proposed by a lot of researchers, mistuning is considered by introducing a different Young's modulus for each blade

$$ E_i = E_0 \left(1 + p_i \right) \tag{8} $$

where E_0 and p_i are Young's modulus for the tuned blade and the dimensionless mistuning parameter for the i$^{\mathrm{th}}$ blade. Assuming this simplistic but sufficient case for the purpose of this study, the variation of the stiffness matrix $\bar{\mathbf{K}}_{\mathbf{bb}}$ due to the mistuned characteristics of each blade is added in $\bar{\mathbf{K}}$ such as

$$ \bar{\mathbf{K}}_{\mathbf{bb}} = diag\left(1 + p_i \right) \otimes \left({}^{\mathrm{b}}\tilde{\boldsymbol{\Psi}} \cdot {}^{\mathrm{b}}\tilde{\mathbf{K}} \cdot {}^{\mathrm{b}}\tilde{\boldsymbol{\Psi}} \right) \tag{9} $$

where $diag(1+p_i)$ defines the diagonal matrix of $(1+p_i)$ coefficients. $\otimes$ defines the Kronecker product.

3 MISTUNING IDENTIFICATION TECHNIQUE

The aim of mistuning identification is to find the mistuning parameters to correct the model (here a reduced order model) so that it properly describes the dynamic behaviour of a real bladed disk. To do so, global measurements of a system of modes are necessary and are taken as a reference. The procedure is similar to model updating techniques.

The method proposed to identify mistuning parameters is based on the Best Achievable Eigenvectors [26-27]. This approach uses an eigenvalue assignment technique combined with a regularization technique and consists in a projection of the measured eigenvectors on a subspace spanned by the perturbed model; this improves the representativeness of the measured modes and limits the influence of measurement errors .

As explained previously, mistuning has been introduced in our model by considering that each blade has different cantilevered frequencies. Perturbation parameters are then applied to the modal coordinates corresponding to the perturbed modes and mistuned reduced stiffness matrix $\bar{\mathbf{K}}_{\mathbf{M}}$ is given by

$$\bar{\mathbf{K}}_{\mathbf{M}} = \bar{\mathbf{K}}_{\mathbf{T}} + \sum_{i=1}^{N} p_i \, {}^{i}\bar{\mathbf{K}} \tag{10}$$

where $\bar{\mathbf{K}}_{\mathbf{T}}$ and ${}^{i}\bar{\mathbf{K}}$ are the tuned matrix and the elementary stiffness matrix of the i^{th} blade (N defines the total number of stiffness element matrix).

The eigenvalue equation associated with the dynamic structural system is

$$\bar{\mathbf{K}}_{\mathbf{M}}\bar{\mathbf{\Psi}}^{r} = \bar{\mathbf{M}}\bar{\mathbf{\Psi}}^{r}\mathbf{\Lambda}^{r} \tag{11}$$

where $\bar{\mathbf{\Psi}}^{r}$ is the r eigenvectors in modal coordinates and and $\mathbf{\Lambda}^{r}$ is a diagonal matrix containing r system eigenvalues.

By substituting equation (9) into equation (10), we have

$$\sum_{i=1}^{N} p_i \, {}^{i}\bar{\mathbf{K}}\bar{\mathbf{\Psi}}^{r} = \bar{\mathbf{M}}\bar{\mathbf{\Psi}}^{r}\mathbf{\Lambda}^{r} - \bar{\mathbf{K}}_{\mathbf{T}}\bar{\mathbf{\Psi}}^{r} \tag{12}$$

This equation will be used in a first time for the eigenvectors regularization and in a second time for the mistuning parameters identification.

Each eigenvector is filtered independently with equation (12) written for each mode j.

$$\sum_{i=1}^{N} p_i \, {}^{i}\bar{\mathbf{K}}\bar{\mathbf{\Psi}}_{j}^{r} = \left(\omega_j^2\bar{\mathbf{M}} - \bar{\mathbf{K}}_{\mathbf{T}}\right)\bar{\mathbf{\Psi}}_{j}^{r} \tag{13}$$

If all measured eigenfrequencies for the mistuned system are different from the ones of the tuned system, each eigenvector can be isolated in the previous equation. Considering the j^{th} mode, the equation (13) is rewritten as

$$\sum_{i=1}^{N} p_i \mathbf{E}_j^{-1} \, {}^{i}\bar{\mathbf{K}}\bar{\mathbf{\Psi}}_{j}^{r} = \bar{\mathbf{\Psi}}_{j}^{r} \tag{14}$$

where

$$\mathbf{E}_j = \left(\omega_j^2\bar{\mathbf{M}} - \bar{\mathbf{K}}_{\mathbf{T}}\right) \tag{15}$$

Equation (14) can now be rewritten as

$$\mathbf{L}_j \boldsymbol{\gamma}_j = \bar{\boldsymbol{\Psi}}_j^r \tag{16}$$

where

$$\mathbf{L}_j = \left[\mathbf{E}_j^{-1\,1}\bar{\mathbf{K}} \quad \mathbf{E}_j^{-1\,2}\bar{\mathbf{K}} \quad \cdots \quad \mathbf{E}_j^{-1\,N}\bar{\mathbf{K}} \right] \tag{17}$$

and

$$\boldsymbol{\gamma}_j = \left[p_1 \bar{\boldsymbol{\Psi}}_j^r \quad \cdots \quad p_N \bar{\boldsymbol{\Psi}}_j^r \right]^T \tag{18}$$

Equation (16) is only true if $\bar{\boldsymbol{\Psi}}_j^r$ is a linear combination of the columns of $\mathbf{L}_j$. In this case, $\bar{\boldsymbol{\Psi}}_j^r$ must lie in the subspace spanned by the columns of $\mathbf{L}_j$ which are only dependent of the tuned system matrices and of the eigenfrequency ω_j. In practice, this equation is not verified because of measurements noise or eventual non-linearities not taken into account in model.

As a consequence, a regularization step is necessary to achieve this condition. This consists in a projection of each measured $\bar{\boldsymbol{\Psi}}_j^r$ onto the subspace spanned by the nonzero columns of $\mathbf{L}_j$. An optimal vector $\boldsymbol{\gamma}_j$ is calculated to satisfy equation $\mathbf{L}_j \boldsymbol{\gamma}_j = \bar{\boldsymbol{\Psi}}_j^r$ as follows

$$\boldsymbol{\gamma}_j = \mathbf{L}_j{}^{+} \bar{\boldsymbol{\Psi}}_j^r \tag{19}$$

where the superscript $^+$ denotes the pseudoinverse of a matrix. In fact, this optimal solution does not give back exactly the measured eigenvector $\bar{\boldsymbol{\Psi}}_j^r$, but a regularized one which is realizable with mistuning parameters values *pi*. This vector $\bar{\boldsymbol{\Psi}}_j^{rf}$ defined as the best achievable eigenvector for j^{th} mode is given by

$$\bar{\boldsymbol{\Psi}}_j^{rf} = \mathbf{L}_j \mathbf{L}_j{}^{+} \bar{\boldsymbol{\Psi}}_j^r \tag{20}$$

Then equation (12) can be rewritten with this best achievable eigenvectors as

$$\sum_{i=1}^{N} p_i{}^{i} \bar{\mathbf{K}} \bar{\boldsymbol{\Psi}}^{rf} = \bar{\mathbf{M}} \bar{\boldsymbol{\Psi}}^{rf} \boldsymbol{\Lambda}^r - \bar{\mathbf{K}}_{\mathbf{T}} \bar{\boldsymbol{\Psi}}^{rf} \tag{21}$$

By rearranging this equation we have

$$\hat{\mathbf{L}}\mathbf{p} = \mathbf{R} \tag{22}$$

where

$$\mathbf{p} = \left\{ p_1 \quad p_2 \quad \cdots \quad p_N \right\}^T \tag{23}$$

and

$$\hat{\mathbf{L}} = \begin{bmatrix} {}^{1}\bar{\mathbf{K}}\bar{\boldsymbol{\Psi}}_1^{rf} & {}^{2}\bar{\mathbf{K}}\bar{\boldsymbol{\Psi}}_1^{rf} & \cdots & {}^{N}\bar{\mathbf{K}}\bar{\boldsymbol{\Psi}}_1^{rf} \\ {}^{1}\bar{\mathbf{K}}\bar{\boldsymbol{\Psi}}_2^{rf} & {}^{2}\bar{\mathbf{K}}\bar{\boldsymbol{\Psi}}_2^{rf} & \cdots & {}^{N}\bar{\mathbf{K}}\bar{\boldsymbol{\Psi}}_2^{rf} \\ \vdots & \vdots & \ddots & \vdots \\ {}^{1}\bar{\mathbf{K}}\bar{\boldsymbol{\Psi}}_r^{rf} & {}^{2}\bar{\mathbf{K}}\bar{\boldsymbol{\Psi}}_r^{rf} & \cdots & {}^{N}\bar{\mathbf{K}}\bar{\boldsymbol{\Psi}}_r^{rf} \end{bmatrix} \tag{24}$$

$$\mathbf{R} = \begin{Bmatrix} \bar{\mathbf{M}}\bar{\boldsymbol{\Psi}}_1^{rf}\omega_1^2 - \bar{\mathbf{K}}_{\mathbf{T}}\bar{\boldsymbol{\Psi}}_1^{rf} \\ \bar{\mathbf{M}}\bar{\boldsymbol{\Psi}}_2^{rf}\omega_2^2 - \bar{\mathbf{K}}_{\mathbf{T}}\bar{\boldsymbol{\Psi}}_2^{rf} \\ \vdots \\ \bar{\mathbf{M}}\bar{\boldsymbol{\Psi}}_r^{rf}\omega_r^2 - \bar{\mathbf{K}}_{\mathbf{T}}\bar{\boldsymbol{\Psi}}_r^{rf} \end{Bmatrix} \tag{25}$$

Finally, the vector $\mathbf{p}$ can be estimated according to a root mean square solution, which gives minimal norm parameters values

$$\mathbf{p} = \hat{\mathbf{L}}^{+}\mathbf{R} \tag{26}$$

4 NUMERICAL VALIDATION ON AN INDUSTRIAL BLISK

In this section, a numerical validation of the mistuning identification procedure previously described will be presented. In Figure 1 an industrial high pressure blisk is presented. This blisk features 72 blades. It has been chosen because measurements of individual blade characteristics are not possible for such structure. Assuming a structure with perfect cyclic symmetry , a finite element model of a single sector, shown in Figure 2, is created to conduct the study: there are 2706 degrees of freedom per sector in the finite element model which corresponds for the entire blisk to 584496 degrees of freedom. From this FE model and using the technique presented in section 2.1, a reduced order model is constructed, which consists of the first cantilevered blade modes and the first disk modes given in Table 1. Finally, it has 295 degrees of freedom (72 modal coordinates for blade modes and 223 for disk modes). This reduced model is validated since perfect correlation are found (all frequency errors are lower than 0.15% with respect to the cyclic symmetry model taken as reference).

With this model, four illustrative examples with various mistuning configurations are presented in order to validate the procedure identification previously described and to check the range of applicability of the technique.

The numerical validation procedure is divided in three main steps. After the choice of a given mistuning pattern for the blisk, mistuned free response is calculated in order to obtain mistuned eigenfrequencies and eigenvectors. These eigenvectors are then limited to one degree-of-freedom per blade in order to simulate punctual experimental measurement and perturbed to represent measurement noise. Secondly, tuned free response of the blisk is calculated in order to access to tuned eigenvectors which are used to expand measured eigenvectors on all physical degree-of-freedom. These vectors can then be reduced in modal coordinates. Finally, updating procedure is applied to estimate mistuning parameters initially imposed.

For this study, we focus on the identification of the first family of modes (here first bending mode); however, the identification could be on any other modes.

The identification approach is checked with the following cases:

- case 1: all the 72 blades' modes of the blisk are available and not perturbed. Mistuning with 2.34% standard deviation and 0% mean is applied.
- case 2: experimentally speaking, it is unprobable that all eigenvectors are identified with modal extraction particularly because the high modal density of such structures. Thus we considered that 62 out of 72 modes are available for the identification. Mistuning with 0% mean and 2.34% standard deviation, and perturbed eigendata (random gaussian perturbation of +/-20% on all components of eigenvectors and of +/-0.15% on all eigenfrequencies) are introduced. This case is closer to the « true mistuning » of a blisk.
- case 3 : 62 modes are available for the identification. Mistuning with 0% mean and 6.18% standard deviation and perturbed eigendata (random gaussian perturbation of +/-20% on all components of eigenvectors and of +/-0.15% on all eigenfrequencies) are introduced. For a blisk, typical mistuning is less than 2%. However, this case is presented in order to check the range of validity of the identification procedure and to validate the method for important mistuning.
- case 4 : 62 modes are available for the identification. The mistuning is modeled as being normally distributed with 20% mean and 2.34% standard deviation. This last case is tested to check the robustness of the identification procedure to modeling errors for example due to wrong evaluations of the coupling between the blades and the disk.

Figures 3, 7,11 and 15 illustrate the correlation between the exact and estimated mistunings for the first, second, third and fourth cases, respectively. The differences between exact and estimated mistuning and the associated relative errors for the four cases are presented in Figures

4, 8, 12 and 16, and 6, 10, 14 and 18, respectively. Figures 5, 9, 13 and 17 illustrate the associated frequency error for each mode.
In all cases, the correlations are excellent. For the first case, the differences between exact and estimated mistuning for each blade is negligible : the relative error inferior to 0.25% and the maximum frequency error inferior to 0.03Hz. Moreover, the correlations are excellent when only 62 of 72 modes are available for the identification (second, third and fourth cases) ; the maximal difference between the exact and estimated moistening is obtained for the third case and is lower than 0.8% for each blade number. The maximum relative error is lower than 15% (obtained for the second case). In all cases, error between eigenfrequencies calculated with exact and estimated mistuning are lower than 2Hz for all modes, although frequencies are around 2000Hz.
This study shows the good performances of the proposed identification technique for different mistuning configuration taking into account measurement errors as well as modeling errors (without 0% mean); furthermore for relatively high values of mistuning, this results are still satisfying.

5 SENSITIVITY ANALYSIS

As mentioned earlier, the performances of model updating methods such as the one presented here are highly influenced by it robustness to measurements errors. In this section, a sensitivity analysis is undertaken in order to evaluate error made on mistuning parameters for a given error on measured data. The objective is to evaluate if the mistuning parameters can be properly updated with usual measurement errors. To do so, we study the sensibility of the mistuning vector $\mathbf{p}$ first to perturbations on measured frequency ω_j and then, to perturbation on the components of the jth modal eigenvector $\bar{\boldsymbol{\Psi}}_j^r$ and eigenvector $\bar{\boldsymbol{\Psi}}_{X_j}$.

5.1 Sensitivity to eigenfrequencies

If ε is the eigenfrequency perturbation such that,

$$\omega_j^{pert} = \omega_j + \varepsilon \tag{27}$$

then, assuming a first order Taylor development, the corresponding mistuning vector $\mathbf{p}$ is perturbed as follows:

$$\mathbf{p}^{pert} = \mathbf{p} + \varepsilon \frac{\partial \mathbf{p}}{\partial \omega_j} \tag{28}$$

The mistuning vector is a function of the regularized measured eigenvectors so are its perturbation and its sensibility. So, we need to express the perturbed regularized measured eigenvectors and their sensitivities.
Noting from equations (15), (17) and (20) that:

$$\left(\frac{\partial \bar{\boldsymbol{\Psi}}_i^{rf}}{\partial \omega_j} \right)_{i \neq j} = \mathbf{0} \tag{29}$$

and performing derivations of each member of the regularized measured eigenvectors (given in (20)) versus ω_j we find the sensitivities:

$$\frac{\partial \bar{\boldsymbol{\Psi}}}{\partial \omega_j} = \frac{\partial \left(\mathbf{L}_j \mathbf{L}_j^{+} \right)}{\partial \omega_j} \bar{\boldsymbol{\Psi}}_j^r = 2\omega_j \left(\mathbf{L}_j \mathbf{L}_j^{+} - \mathbf{I} \right) \mathbf{E}_j^{-1} \bar{\mathbf{M}} + 2\omega_j \mathbf{L}_j \mathbf{L}_j^{+} \bar{\mathbf{M}} \mathbf{E}_j^{-1} \left(\bar{\boldsymbol{\Psi}}_j^f - \bar{\boldsymbol{\Psi}}_j^r \right) \tag{30}$$

For $\omega_j^{pert} = \omega_j + \varepsilon$, we have with a first order development for regularized measured eigenvectors:

$$\overline{\boldsymbol{\Psi}}_j^{rf\ pert} = \overline{\boldsymbol{\Psi}}_j^{rf} + \varepsilon \frac{\partial \overline{\boldsymbol{\Psi}}_j^{rf}}{\partial \omega_j} = \overline{\boldsymbol{\Psi}}_j^{rf} + \varepsilon \overline{\boldsymbol{\Psi}}_{j,j}^{rf} \tag{31}$$

Introducing, the perturbed expressions of p and $\boldsymbol{\psi}$ in Equation (22) we can write

$$\left(\hat{\mathbf{L}} + \varepsilon \mathbf{J}\right)\mathbf{p}^{pert} = \mathbf{R} + \mathbf{R}_1 \tag{32}$$

where

$$\mathbf{J} = \begin{bmatrix} \mathbf{0} & \cdots & \mathbf{0} \\ \vdots & & \vdots \\ {}^1\overline{\mathbf{K}}\overline{\boldsymbol{\Psi}}_{j,j}^{rf} & \cdots & {}^N\overline{\mathbf{K}}\overline{\boldsymbol{\Psi}}_{j,j}^{rf} \\ \vdots & & \vdots \\ \mathbf{0} & \cdots & \mathbf{0} \end{bmatrix} \tag{33}$$

$$\mathbf{R}_1 \ddot{} = \begin{Bmatrix} \mathbf{0} \\ \vdots \\ \left(\omega_j^2 \overline{\mathbf{M}} - \overline{\mathbf{K}}_{\mathbf{T}}\right)\overline{\boldsymbol{\Psi}}_{j,j}^{rf} + 2\omega_j \overline{\mathbf{M}}\overline{\boldsymbol{\Psi}}_j^{rf} \\ \vdots \\ \mathbf{0} \end{Bmatrix} \tag{34}$$

Noting that $\hat{\mathbf{L}}^t\mathbf{J}$ is symmetric $\left(\hat{\mathbf{L}}^t\mathbf{J} = \mathbf{J}^t\hat{\mathbf{L}}\right)$, we finally have :

$$\frac{\partial \mathbf{p}}{\partial \omega_j} = \hat{\mathbf{L}}^+\mathbf{R}_1 + \left[\left(\hat{\mathbf{L}}^t\hat{\mathbf{L}}\right)^{-1}\mathbf{J}^t - 2\hat{\mathbf{L}}^{-1}\mathbf{J}\hat{\mathbf{L}}^+\right]\mathbf{R} \tag{35}$$

it may be observed that this sensitivity of mistuning parameters to perturbations on eigenfrequencies is dependent of the model and of the mode considered.

5.2 Sensitivity to modal eigenvectors

Mistuning coefficients are identified after reduction of the equations in modal domain. So in a first attempt, we will evaluate the influence of perturbations on the components of the eigenvectors in modal coordinates. As for eigenfrequencies, we impose a perturbation vector $\overline{\boldsymbol{\varepsilon}}$ of components $\overline{\varepsilon}_i$ (for $i = 1,\cdots,\overline{n}$ where $\overline{n}$ is the total number of modal coordinates) to the j^{th} non-regularized eigenvector

$$\overline{\boldsymbol{\Psi}}_j^{r\ pert} = \overline{\boldsymbol{\Psi}}_j^{r} + \overline{\boldsymbol{\varepsilon}} \tag{36}$$

We will consider the following notations

$$\overline{\boldsymbol{\varepsilon}} = \sum_{i=1}^{\overline{n}} \overline{\varepsilon}_i \mathbf{C}_i \tag{37}$$

where $\mathbf{C}_i$ is a zero vector expect for the i^{th} term egals 1.
From equation (20), expression of the perturbed filtered eigenvector takes the form

$$\overline{\boldsymbol{\Psi}}_j^{rf\ pert} = \mathbf{L}_j\mathbf{L}_j^{+}\overline{\boldsymbol{\Psi}}_j^{r\ pert} = \overline{\boldsymbol{\Psi}}_j^{rf} + \mathbf{L}_j\mathbf{L}_j^{+}\overline{\boldsymbol{\varepsilon}} \tag{38}$$

By taking into account the perturbed expression of equation (38), equation (22) can be written as

$$\hat{\mathbf{L}}^{pert}\mathbf{p}^{pert} = \mathbf{R}^{pert} \tag{39}$$

where

$$\hat{\mathbf{L}}^{pert} = \hat{\mathbf{L}} + \sum_{i=1}^{\bar{n}} \bar{\boldsymbol{\varepsilon}}_i \begin{bmatrix} \mathbf{0} & \cdots & \mathbf{0} \\ \vdots & & \vdots \\ {}^{1}\bar{\mathbf{K}}\mathbf{L}_j\mathbf{L}_j{}^{+}\mathbf{C}_i & \cdots & {}^{N}\bar{\mathbf{K}}\mathbf{L}_j\mathbf{L}_j{}^{+}\mathbf{C}_i \\ \vdots & & \vdots \\ \mathbf{0} & \cdots & \mathbf{0} \end{bmatrix} = \hat{\mathbf{L}} + \sum_{i=1}^{\bar{n}} \bar{\boldsymbol{\varepsilon}}_i \hat{\mathbf{L}}_i \tag{40}$$

Considering a first order development, equation (26) has the following form

$$\mathbf{p}^{pert} \approx \mathbf{p} + \sum_{i=1}^{\bar{n}} \bar{\boldsymbol{\varepsilon}}_i \frac{\partial \mathbf{p}}{\partial \bar{\boldsymbol{\varepsilon}}_i} \tag{41}$$

Noting that $\hat{\mathbf{L}}^t\hat{\mathbf{L}}_i$ is symmetric, we finally have

$$\frac{\partial \mathbf{p}}{\partial \bar{\boldsymbol{\varepsilon}}_i} = \hat{\mathbf{L}}^{+}\mathbf{R}_i + \left[\left(\hat{\mathbf{L}}^t\hat{\mathbf{L}} \right)^{-1} \hat{\mathbf{L}}_i^t - 2\hat{\mathbf{L}}^{+}\hat{\mathbf{L}}_i\hat{\mathbf{L}}^{+} \right] \mathbf{R} \tag{42}$$

This expression is quite similar to the one obtained for perturbations on eigenfrequencies by making the correspondence between $\mathbf{J}$ and $\hat{\mathbf{L}}_i$ and between $\mathbf{R}_1$ and $\mathbf{R}_i$.

5.3 Sensitivity to measured eigenvectors

In practice, measurement error is committed on measured components of eigenvectors in physical coordinates. Thus, we are now going to evaluate sensibility to these coordinates in a second time thanks to previous development made for modal eigenvectors. This way to proceed improves CPU time and used memory. We will note $\boldsymbol{\varepsilon}_X$ the perturbation vector applied on the *j th* eigenvector identified on the n_m measured dof.

$$\bar{\boldsymbol{\psi}}_{X_j}{}^{pert} = \bar{\boldsymbol{\psi}}_{X_j} + \boldsymbol{\varepsilon}_X \tag{43}$$

This vector $\boldsymbol{\varepsilon}_X$ can be linked to $\bar{\boldsymbol{\varepsilon}}$ thanks to matrix $\mathbf{T}_\mathbf{E}$ used for expansion on the *n* physical degrees of freedom of the finite element model, and to matrix $\mathbf{T}$ used for the modal reduction

$$\bar{\boldsymbol{\varepsilon}} = \mathbf{T}^{+}\mathbf{T}_\mathbf{E}\boldsymbol{\varepsilon}_X \tag{44}$$

For the i^{th} component :

$$\bar{\boldsymbol{\varepsilon}}_i = \sum_{k=1}^{n_m} \mathbf{T}^{+}\mathbf{T}_\mathbf{E}(i,k)\boldsymbol{\varepsilon}_{X_k} \tag{45}$$

By considering equations (41) and (45), we can write :

$$\mathbf{p}^{pert} = \mathbf{p} + \sum_{i=1}^{n_m} \boldsymbol{\varepsilon}_{X_k} \frac{\partial \mathbf{p}}{\partial \boldsymbol{\varepsilon}_{X_k}} \tag{46}$$

where

$$\frac{\partial \mathbf{p}}{\partial \boldsymbol{\varepsilon}_{X_k}} = \sum_{k=1}^{\bar{n}} \mathbf{T}^{+}\mathbf{T}_\mathbf{E}(i,k) \frac{\partial \mathbf{p}}{\partial \bar{\boldsymbol{\varepsilon}}_i} \quad \text{with} \quad k = 1,\cdots,n_m \tag{47}$$

6 NUMERICAL RESULTS OF SENSITIVITY ANALYSIS

In this section, the second configuration of mistuning defined in section 4 is used to appreciate sensibility of estimated parameters to measurement errors (62 out of 72 modes are available for the identification ; mistuning with 0% mean and 2.34% standard deviation, and perturbed eigendata: random gaussian perturbation of +/-20% on all components of eigenvectors and of +/-0.15% on all eigenfrequencies). As explained previously, this sensitivity analysis is investigated by calculating expressions (35) and (47).

Results of sensibility to eigenfrequencies and modal eigenvectors are represented on Figures 19 and 20, respectively.
It may be observed that sensibility coefficients are dependent on the mode and the parameter considered. This can be useful to select some modes which are less affected by measurement errors or to give some confidence in results obtained.
Characteristics values are given in Table 2 (by considering modal expansion): maximal value which is to be retained for errors committed on mistuning parameters and mean value to highlight the fact that sensibility is highly dependent of the modes and parameters. They correspond to amplification factors between errors committed on measured eigendata and errors associated to mistuning identified parameters. If errors on identified parameters are of the same level as mistuning for errors committed on experimental data, then a good identification becomes impossible.
At the first glance, maximal sensibility is 100 times greater for eigenfrequencies than for eigenvectors. Identification method is also far more sensitive to errors on frequencies than on eigenvectors. However, errors are not of the same amount for these two kinds of data. If we consider +/-0.15% perturbations for eigenfrequencies and +/-20% for eigenvectors, multiplication with amplification factors given in table 2 gives respectively for mistuning errors +/-0.1514% and +/-0.1679%. So it is approximately of the same level. We can notice the fact that if we calculate maximal sensibility for all degree-of-freedom of eigenvectors, it is greater than the one for measured degree-of-freedom. It implies that expansion procedure should be as precise as possible in order to reduce error amplification.

7 CONCLUSION

A method for mistuning identification in bladed disk has been presented, which is based on an eigendata assignment method coupled with a regularisation of the measured eigenvectors.
The assessment of the identification technique is validated numerically from a finite reduced order element model of an industrial blisk. The validation of this technique was achieved through four numerical validations in order to assess the sensibility of various mistuning. In all cases, it was found good correlation between the estimated and exact mistunings. These results show that this identification technique may provide a valuable tool for predicting mistuning of experimental data for mistuned industrial bladed disks. Besides sensibility analysis has been carried on. It allows to give confidence level in the identified parameters for given errors on experimental data. It can also be used to know if a quality identification can be obtained.

ACKNOWLEDGMENT

Thanks go to SNECMA Moteurs for its financial and technical support in this study.

ANNEXE A: CYCLIC SYMMETRY

Assuming perfect cyclic symmetry for turbomachinery rotors and the properties of circulant matrices and their eigenvectors, a reduced order model formulation reducing the vibration analysis to that of one blade with the corresponding disk sector is commonly applied in order to study the whole structure.

All cyclic symmetry structures have structural matrices which are diagonalisable by the Fourier matrix $\mathbf{E}$ defined by

$$\mathbf{E} = \left(1/\sqrt{N}\right)\begin{bmatrix} 1 & 1 & 1 & \cdots & 1 \\ 1 & \omega & \omega^2 & \cdots & \omega^{N-1} \\ \cdots & \cdots & & & \\ 1 & \omega^{N-1} & \omega^{2(N-1)} & \cdots & \omega^{(N-1)(N-1)} \end{bmatrix} \tag{48}$$

where

$$\omega = e^{\frac{2j\pi}{N}} \qquad \text{and} \qquad j^2 = -1 \tag{49}$$

N defines the dimension of the circulant matrices. Note that $\mathbf{E}$ is orthonormal such that

$$\mathbf{E}^*\mathbf{E} = \mathbf{I} \tag{50}$$

where * defines the complex conjugate transpose.

All circulant matrices of dimension N have the same set of eigenvectors that can be the columns of the Fourier matrix $\mathbf{E}$. Then, all eigenvector $\mathbf{u_i}$ of the whole blisk can be determined from the associated eigenvector $\tilde{\mathbf{u}}_\mathbf{i}$ of one blade with the corresponding disk sector

$$\mathbf{u_i} = \mathbf{e_i} \otimes \tilde{\mathbf{u}}_\mathbf{i} \tag{51}$$

where $\otimes$ defines the Kronecker product and $\mathbf{e_i}$ is the i^{th} column of $\mathbf{E}$.

REFERENCES

1- Ewins, D. J., 1976, "Vibration Modes of Mistuned Bladed Disks," *ASME Journal of Engineering for Power*, Vol. 98, No. 3, pp. 349–355.

2- Srinivisan A.V., 1997, "Flutter and Resonant Vibration Characteristics of Engine Blades », *Journal of Engineering for gas Turbines and Power*, Vol. 119(2), pp. 742-775.

3- Slater J.C., Minkiewicz G.R., Blair A.J., 1999, "Forced Response of Bladed Disk Assemblies - A Survey", *The Shock and Vibration Digest*, Vol. 31(1), pp. 17-24.

4- Ewins D.J., 1969, "The Effects of Detuning upon the Forced Vibrations of Bladed Disks", *Journal of Sound and Vibration*, Vol. 9(1), pp. 65-79.

5- Whitehead D., 1966, "Effect of Mistuning on the Vibration of Turbomachine Blades Induced by Wakes", *Journal of Mechanical Engineering Science*, Vol. 8, pp. 15-21.

6- El-Bayoumy, L. E. and Srinivasan, A. V., 1975, "Influence of Mistuning on Rotor-Blade Vibrations," *AIAA Journal*, Vol. 13, No. 4, pp. 460–464.

7- Balmès E., 1993, "High Modal Density, Curve Veering, Localization: a Different Perspective on the Structural Response", *Journal of Sound and Vibration*, Vol. 161(2), pp. 358-363.

8- Pierre C., 1988, "Mode Localization and Eigenvalue Loci Veering Phenomena in Disordered Structures", *Journal of Sound and Vibration*, Vol. 126(3), pp. 485-502.

9- Wei, S. T. and Pierre, C., 1988a, "Localization Phenomena in Mistuned Assemblies with Cyclic Symmetry, Part I: Free Vibrations," *ASME Journal of Vibration, Acoustics, Stress, and Reliability in Design*, Vol. 110, No. 4, pp. 429–438.

10- Kruse M.J., Pierre C., 1997, "An Experimental Investigation of Vibration Localization in Bladed Disks, Part II : Forced Response", In *Proceedings of the* 42*nd ASME Gas Turbine and Aeroengine Congress, Exposition and Users Symposium*, Orlando, Florida, USA.
11- Castanier M.P., Pierre C., 1997, "Consideration on the Benefits of Intentional Blade Mistuning for the Forced Response of Turbomachinery Rotors", In *Analysis and Design Issues for Modern Aerospace Vehicles*, ASME Publication AD-Vol.55, pp. 419-425.
12- Wei, S. T. and Pierre, C., 1988b, "Localization Phenomena in Mistuned Assemblies with Cyclic Symmetry, Part II: Forced Vibrations,"*ASME Journal of Vibration, Acoustics, Stress, and Reliability in Design*,Vol. 110, No. 4, pp. 439–449.
13- Sinha A., 1986, "Calculating the Statistics of Forced Response of a Mistuned Bladed Disk Assembly", *AIAA Journal*, Vol. 24(11), pp. 1797-1801.
14- Lin C.C., Mignolet M.P., 1996, "Effects of Damping and Damping Mistuning on the Forced Vibration Response of Bladed Disks", *Journal of Sound and Vibration*, Vol. 193(2), pp. 525-543.
15- Seinturier E., Dupont C., Berthillier M., Dumas M., 2000, A New Method to Predict Flutter in Presence of Structural Mistuning, *ISUAAAT 2000*, Lyon, France, September 4-8.
16- Valero, N. A. and Bendiksen, O. O., 1986, "Vibration Characteristics of Mistuned Shrouded Blade Assemblies," *ASME Journal of Engineering for Gas Turbines and Power*, Vol. 108, pp. 293–299.
17- Mignolet M.P., Lin C.C., 1997, "Identification of Structural Parameters in Mistuned Bladed Disks", *Journal of Vibration and Acoustics*, Vol. 119(3), pp. 428-438.
18- Judge, J. A., Pierre, C., and Ceccio, S. L., 2001, "Experimental Validation of Mistuning Identification Techniques and Vibration Predictions in Bladed Disks", *Proceedings of the International Forum on Aeroelasticity and Structural Dynamics-IFASD 2001*, Madrid, Spain.
19- Judge, J. A., Pierre, C., Ceccio, S. L., and Castanier, M. P., 2002, "Experimental Investigation of theeffects of Random and Intentional Mistuning on the Vibration of Bladed Disks", *Proceedings of the 7th National Turbine Engine High Cycle Fatigue Conference*, Palm Beach Gardens, FL.
20- Castanier, M. P., Ottarsson, G, and Pierre, C., 1997, "A Reduced-Order Modeling Technique for Mistuned Bladed Disks", Journal of Vibration and Acoustics, 119, pp. 439 – 447.
21- Bladh, R., Castanier, M. P., and Pierre, C., 2001, "Component-Mode-Based Reduced Order Modeling Techniques for Mistuned Bladed Disks—Part II: Application," ASME Journal of Engineering for Gas Turbines and Power, 123, pp. 100–108.
22- Pichot, F., Thouverez, F., Jezequel, L., and Seinturier, E., 2001, "Mistuning Parameters Identification of a Bladed Disk", Key Engineering Materials, 204 – 205, pp. 123 – 132.
23- Judge, J. A., Pierre, C., and Ceccio, S. L., 2002, "Mistuning Identification in Bladed Disks", *Proceedings of International Conference on Structural Dynamics Modeling*, Madeira Island, Portugal.
24- Kim, N. E., and Griffin, J. H., 2003, "System Identification in Higher Modal Density Regions of Bladed Disks", *Proceedings of the 8th National Turbine Engine High Cycle Fatigue Conference*, Monterey, CA.
25- Feiner, D. M., and Griffin, J. H., 2003, "A Completely Experimental Method of Mistuning Identification in Integrally Bladed Rotors", *Proceedings of the 8th National Turbine Engine High Cycle Fatigue Conference*, Monterey, CA.
26- Lim T.W., Kashangaki T.A.L., 1994, "Structural Damage Detection of Space Truss Structures Using Best Achievable Eigenvectors", *AIAA Journal*, Vol. 32(5), pp. 1049-1057.
27- Lim T.W., 1995, "Structural Detection Using Constrained Eigenstructure Assignment", *Journal of Guidance, Control, and Dynamics*, Vol. 18(3), pp. 411-418.

28- Bladh, R., Castanier, M. P., and Pierre, C., 1999, "Reduced Order Modeling and Vibration Analysis of Mis-tuned Bladed Disk Assemblies with Shrouds," ASME Journal of Engineering for Gas Turbines and Power, 121, pp. 515–522.
29- Bladh, R., Castanier, M. P., and Pierre, C., 2001, "Component-Mode-Based Reduced Order Modeling Techniques for Mistuned Bladed Disks – Part I: Theoretical Models", ASME Journal of Engineering for Gas Turbine and Power, 123, pp. 89 – 99.
30- Feiner D.M., Griffin J.H., 2002, « A Fundamental Model of Mistuning for a Single Family of Modes », Journal of Turbomachinery, Vol. 124, pp. 597-605.
31- Yang, M.-T. and Griffin, J. H., 1997, "A Reduced Order Approach for the Vibration of Mistuned Bladed Disk Assemblies," *ASME Journal of Engineering for Gas Turbines and Power*, Vol. 119, pp. 161–167.
32- Yang, M.-T., and Griffin, J. H., 2001, "A Reduced Order Model of Mistuning Using a Subset of Nominal System Modes," Journal of Engineering for Gas Turbines and Power, **123**(4), pp. 893–900.
33- Feiner, D. M., and Griffin, J. H., 2002, "A Fundamental Model of Mistuning for a Single Family of Modes", ASME Journal of Turbomachinery, 124, pp. 597 – 605.
34- Géradin M., Rixen D., 1993, "Théorie des Vibrations – Application à la dynamique des structures", MASSON.
35- Craig R.R., Bampton M.C.C., 1968, "Coupling of Substructures for Dynamic Analysis", *AIAA Journal*, Vol. 6(7), pp. 1313-1319.
36- Lim, S., Bladh, R., Castanier, M. P., and Pierre, C., 2003, "A Compact, Generalized Component Mode Mistuning Representation for Modeling Bladed Disk Vibration," AIAA Paper 2003-1545, *Proceedings of the 44th AIAA/ASME/ASCE/AHS Structures, Structural Dynamics, and Materials Conference*, 2, pp. 1359−1380.
37- Benfield, W.A., and Hruda, R.F., 1971, "Vibration analysis of Strucutres by Component Mode Substitution", *AIAA Journal*, Vol. 6, pp. 1313-1919.

Nodal diameter	Number of disk modes retained
0	6
1	7
2	10
3	10
4	10
5	10
6	9
7	8
8	7
9	7
10	4
11	2
12	1
13	1
⋮	⋮
36	1

Table 1 : retained disk modes

Sensitivity	maximal	mean
for eigenfrequencies	1.009644	0.017605
for measured dof of eigenvectors	0.008395	0.000009

Table 2 : characteristics values of sensitivity

Figure 1: industrial blisk

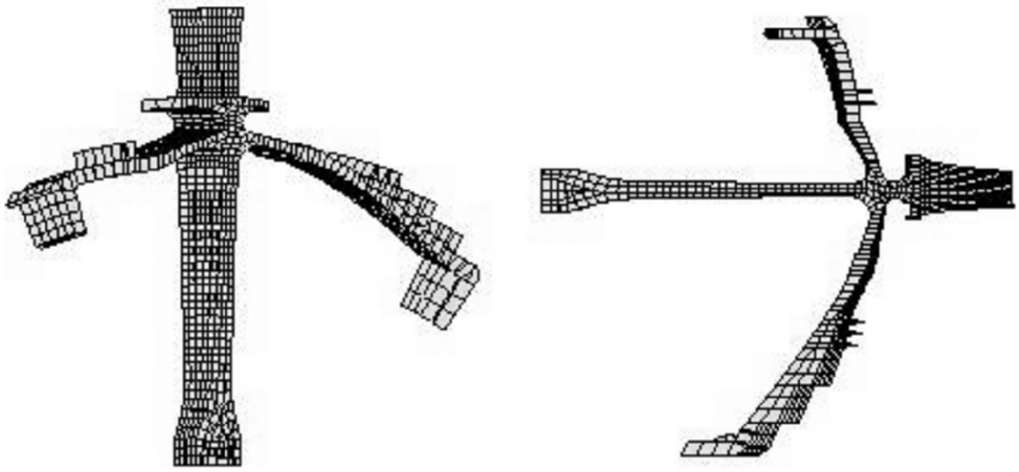

Figure 2: finite element model of a blisk sector

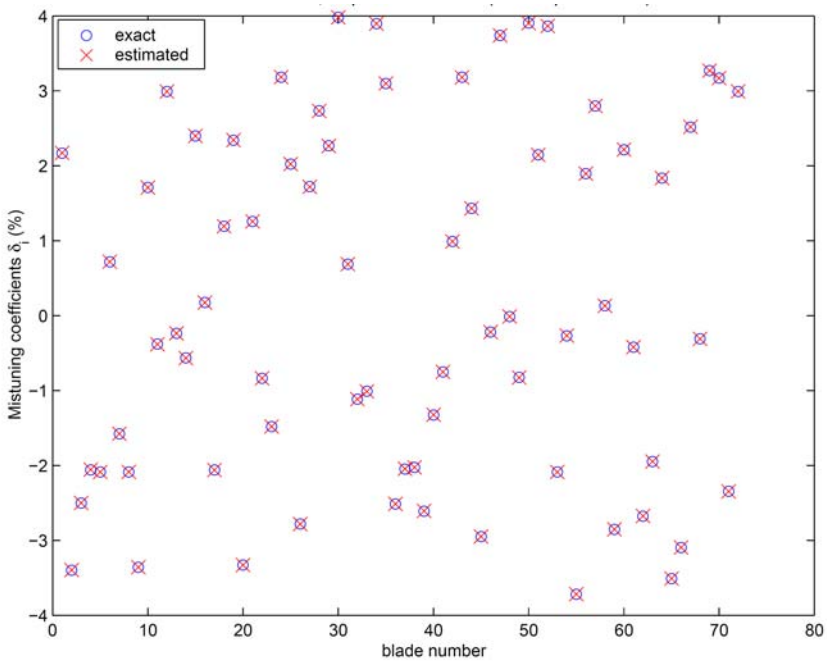

Figure 3: exact and estimated mistuning (case 1: all the 72 blades' modes of the blisk are available, 2.34% standard deviation and 0% mean)

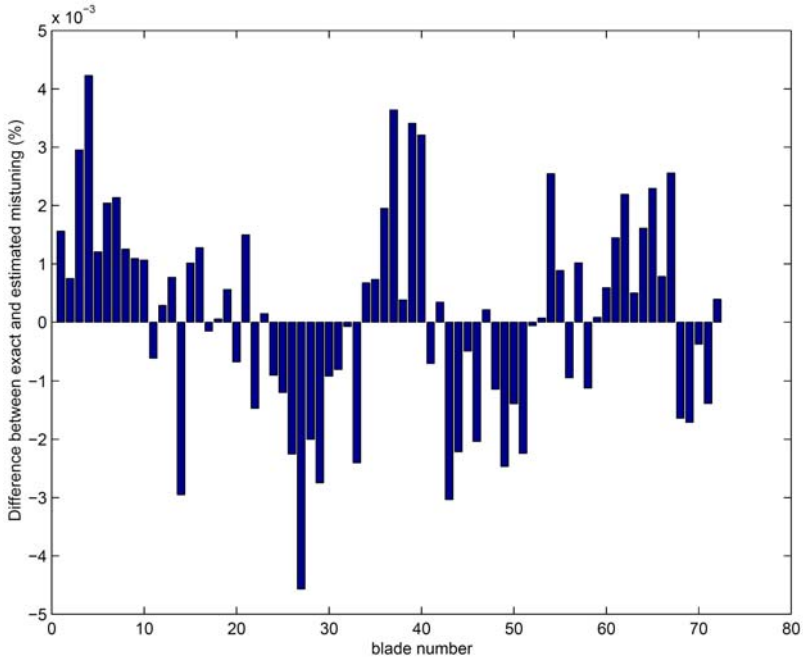

Figure 4: difference between exact and estimated mistuning (case 1: all the 72 blades' modes of the blisk are available, 2.34% standard deviation and 0% mean)

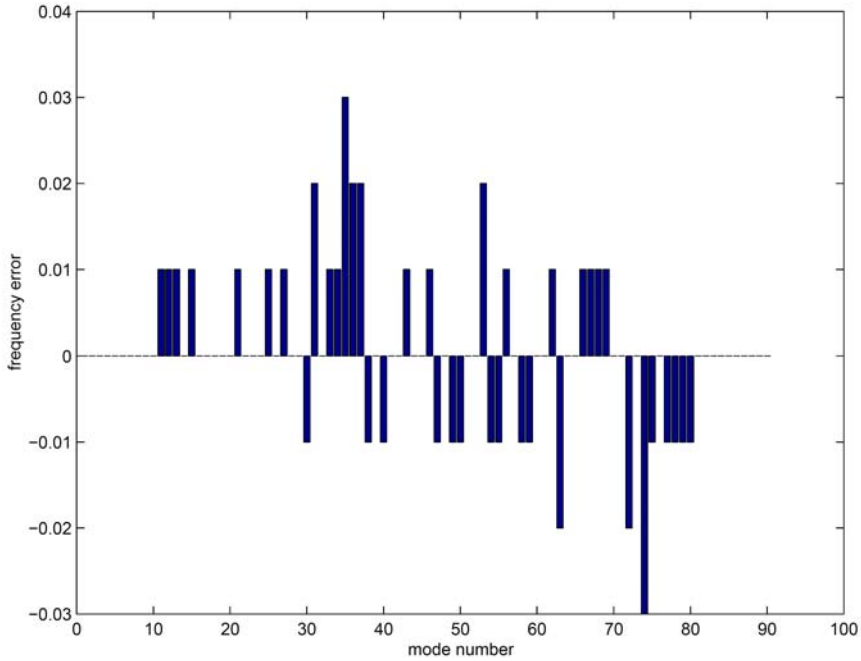

Figure 5: frequency error (case 1: all the 72 blades' modes of the blisk are available, 2.34% standard deviation and 0% mean)

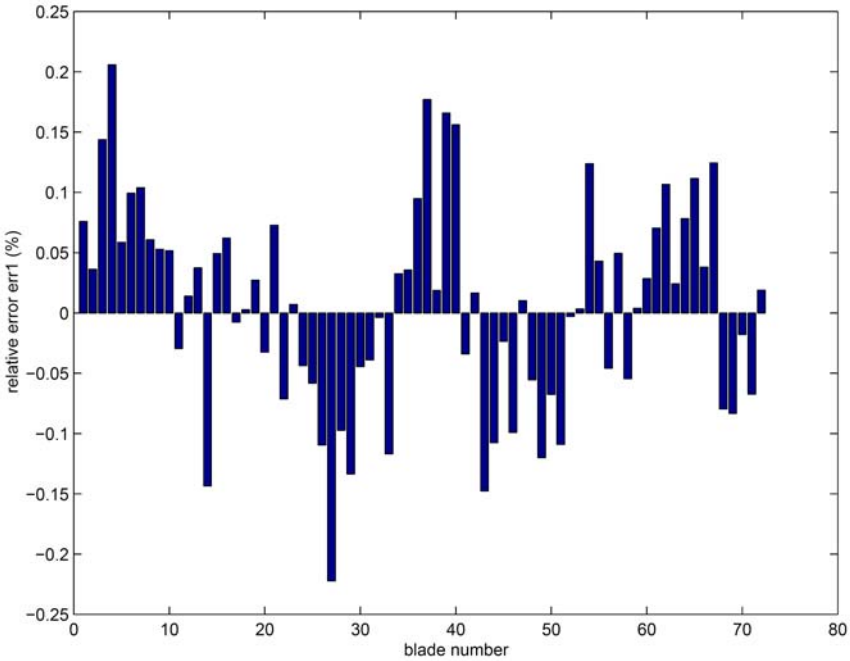

Figure 6: relative error (case 1: all the 72 blades' modes of the blisk are available, 2.34% standard deviation and 0% mean)

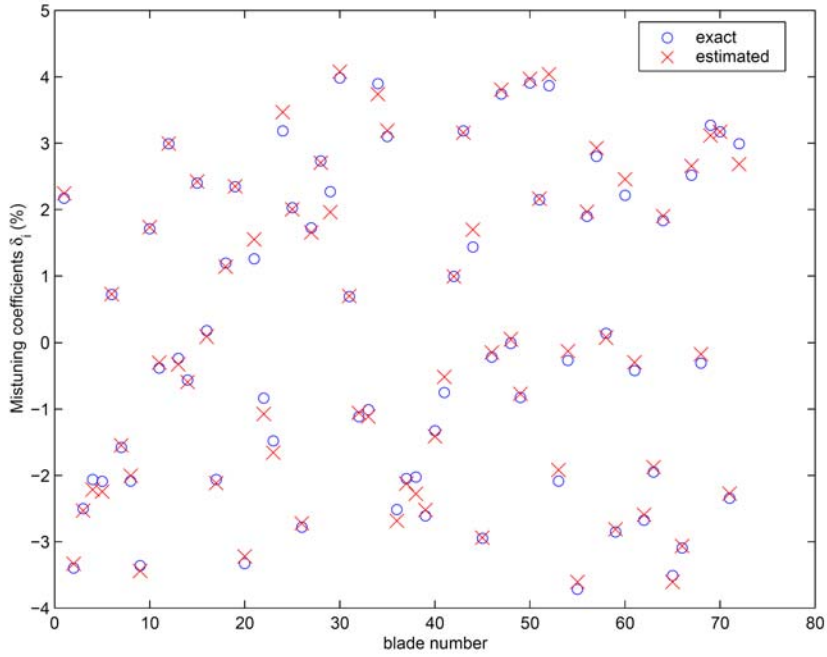

Figure 7: exact and estimated mistuning (case 2: 62 measured modes, 0% mean and 2.34% standard deviation)

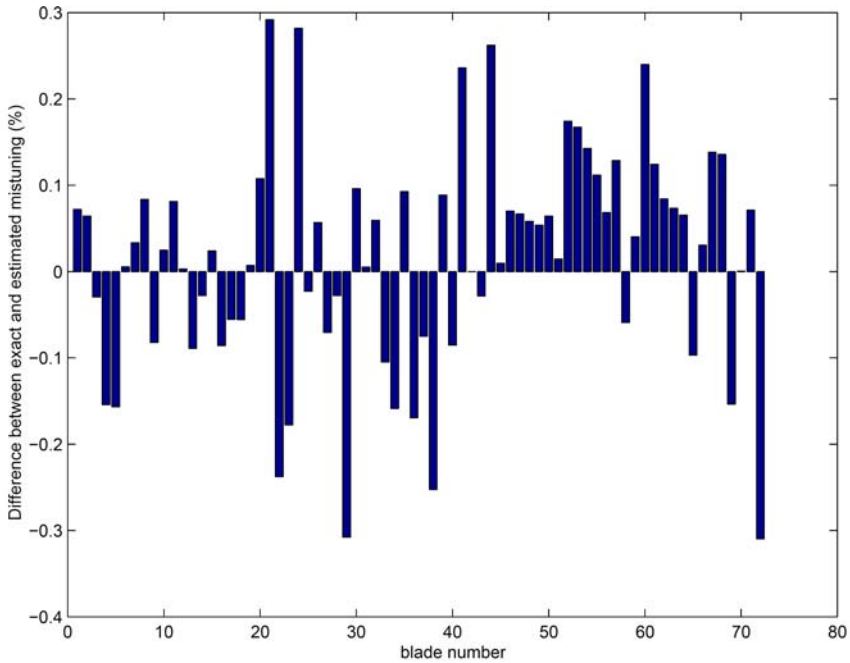

Figure 8: difference between exact and estimated mistuning (case 2: 62 measured modes, 0% mean and 2.34% standard deviation)

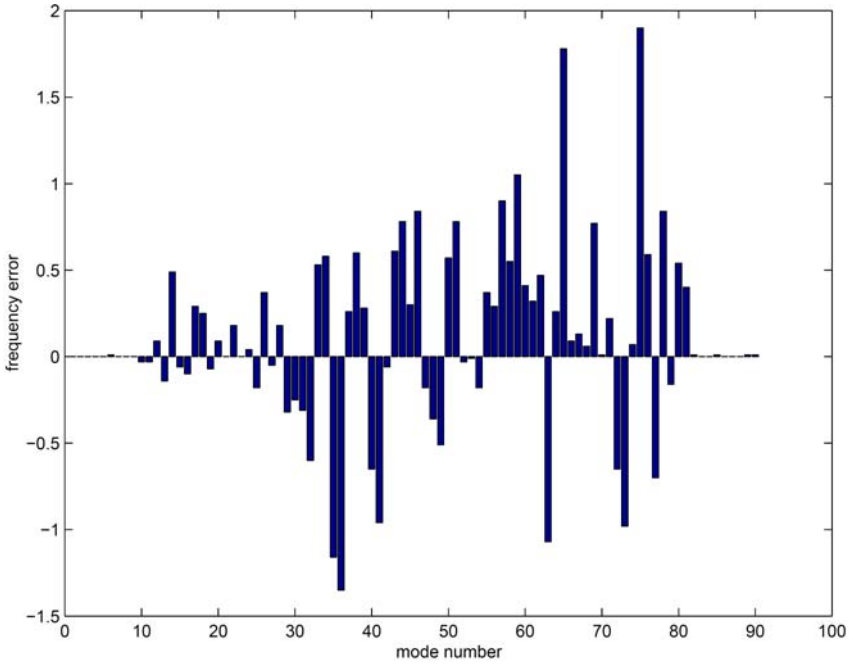

Figure 9: frequency error (case 2: 62 measured modes, 0% mean and 2.34% standard deviation)

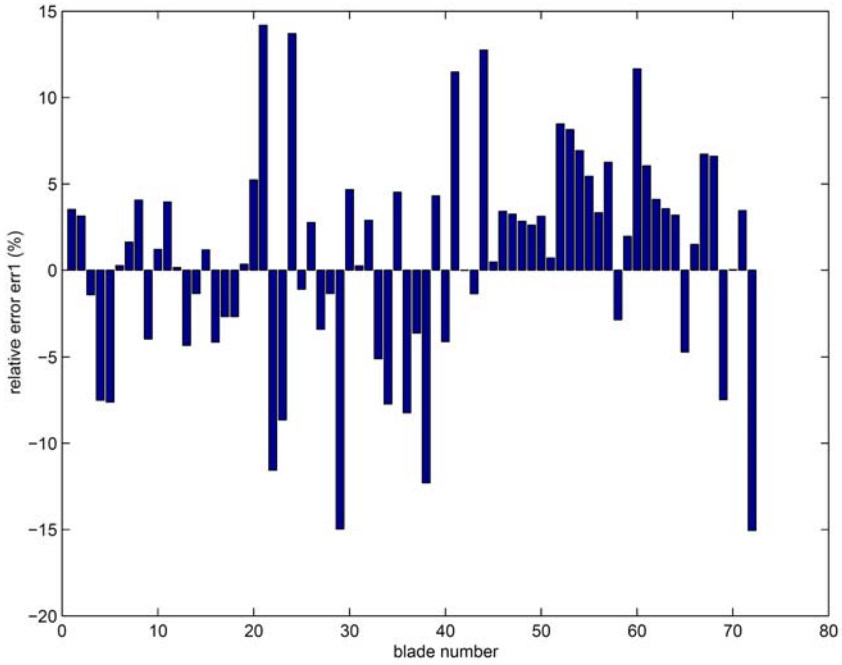

Figure 10: relative error (case 2: 62 measured modes, 0% mean and 2.34% standard deviation)

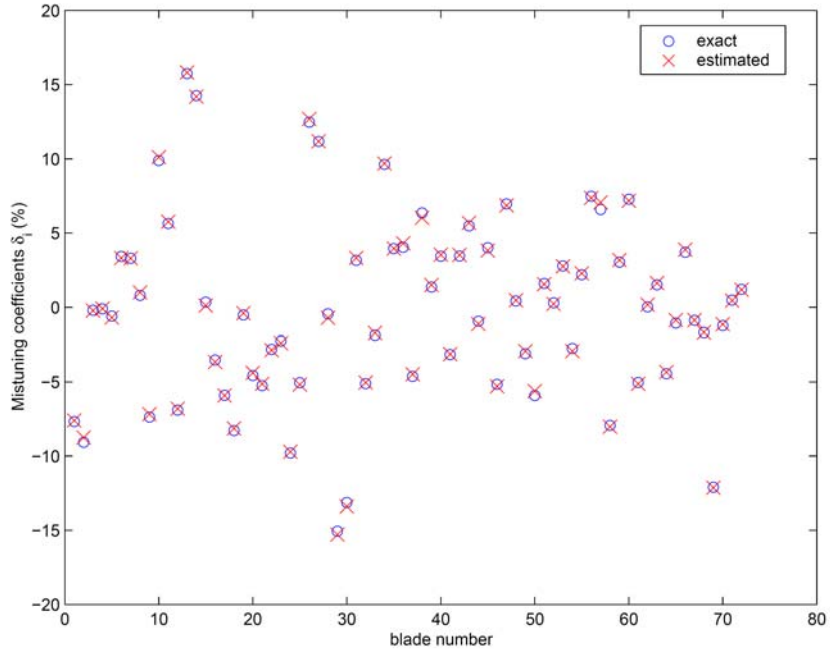

Figure 11: exact and estimated mistuning (case 3: 62 measured modes,0% mean and 6.18% standard deviation)

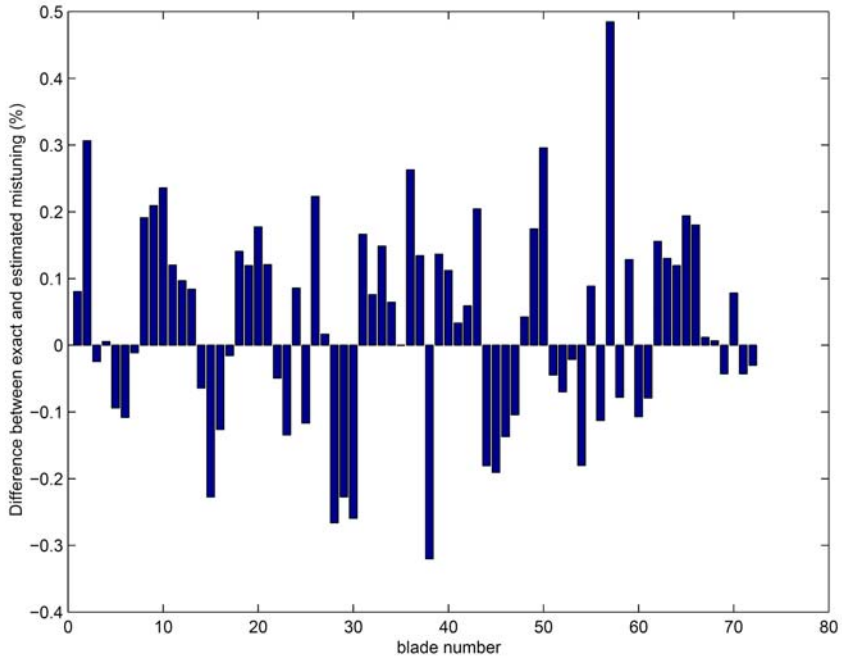

Figure 12: difference between exact and estimated mistuning (case 3: 62 measured modes,0% mean and 6.18% standard deviation)

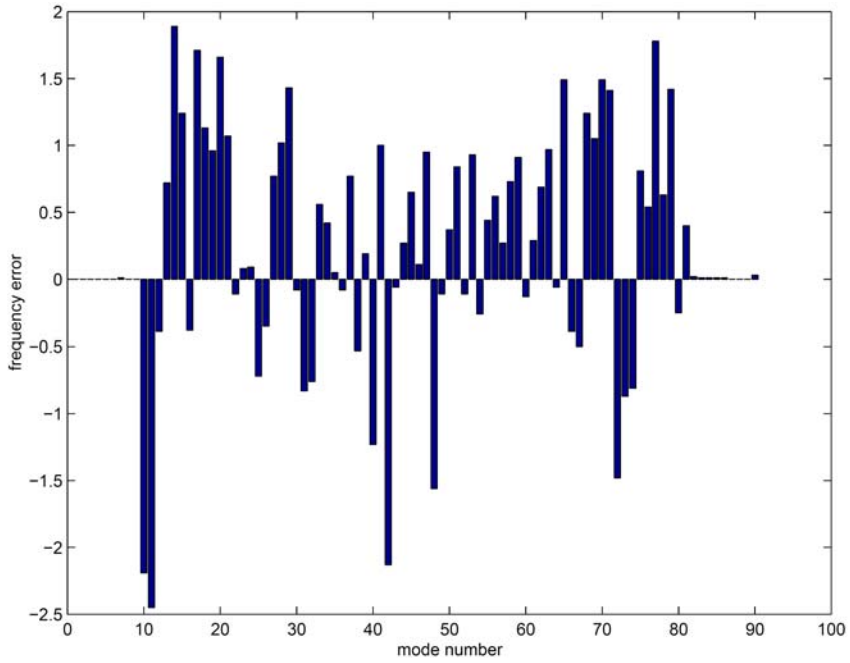

Figure 13: frequency error (case 3: 62 measured modes,0% mean and 6.18% standard deviation)

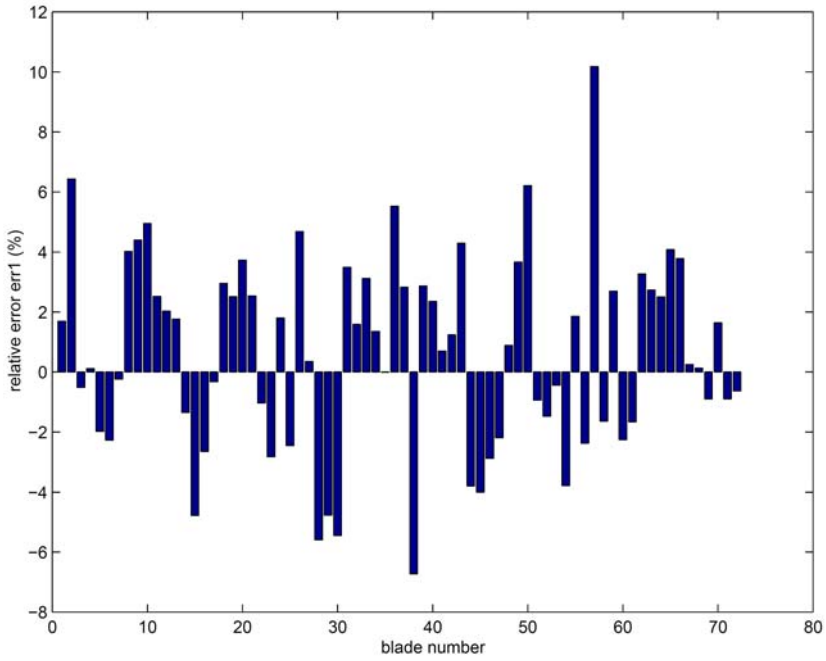

Figure 14: relative error (case 3: 62 measured modes,0% mean and 6.18% standard deviation)

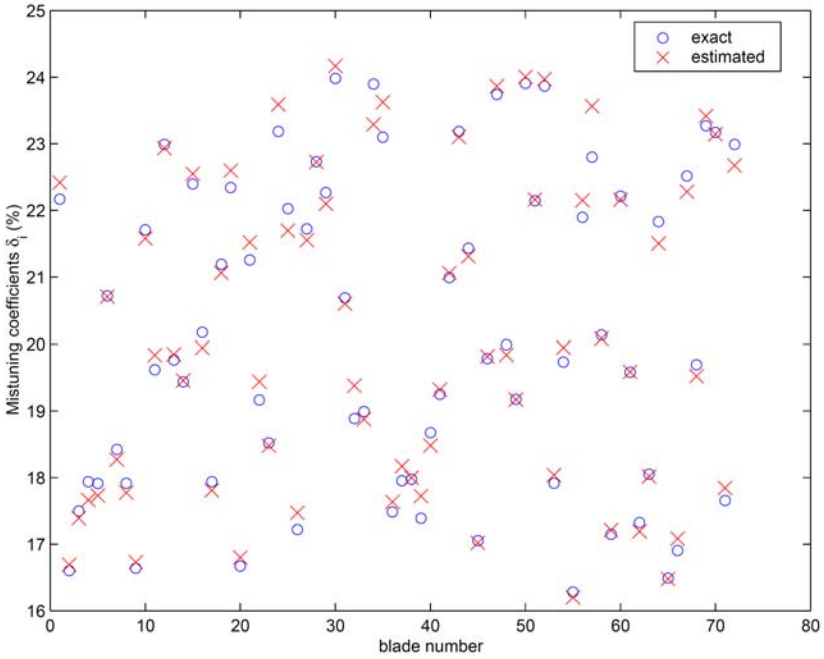

Figure 15: exact and estimated mistuning (case 4: 62 measured modes, 20% mean and 2.34% standard deviation)

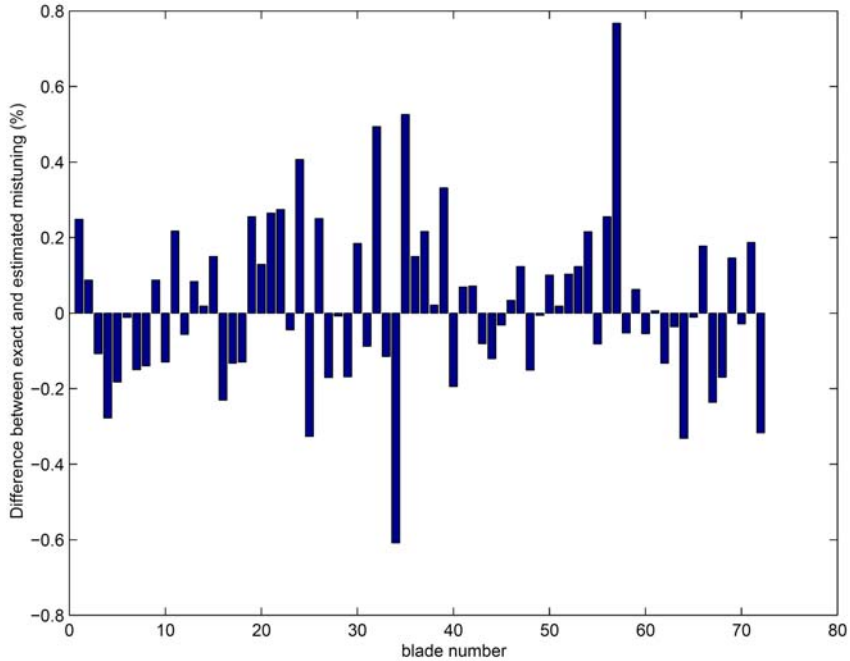

Figure 16: difference between exact and estimated mistuning (case 4: 62 measured modes, 20% mean and 2.34% standard deviation)

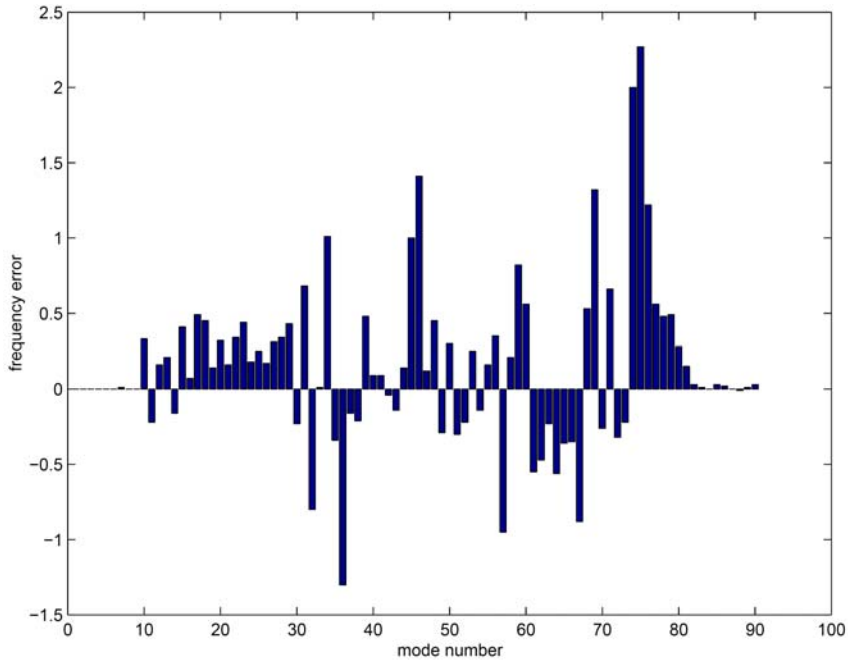

Figure 17: frequency error (case 4: 62 measured modes, 20% mean and 2.34% standard deviation)

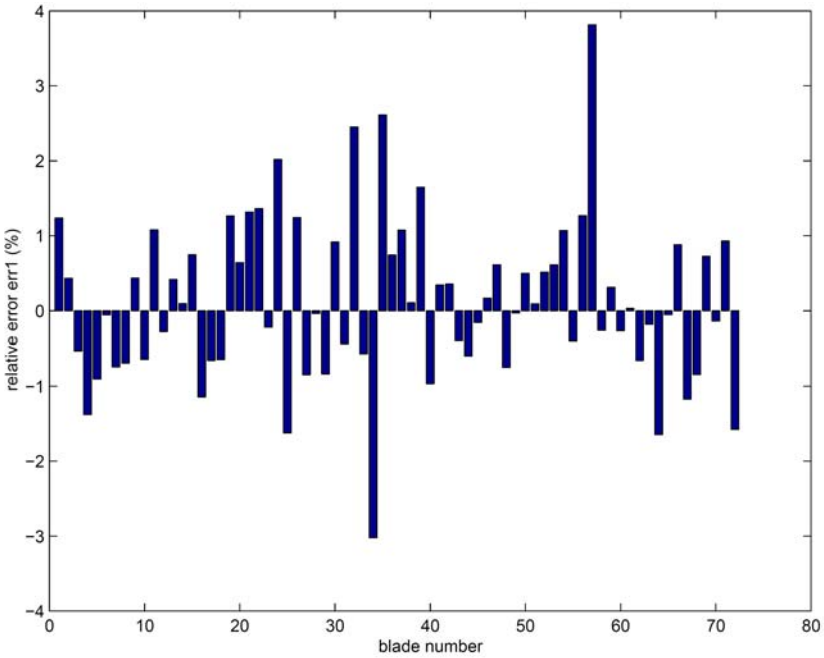

Figure 18: relative error (case 4: 62 measured modes, 20% mean and 2.34% standard deviation)

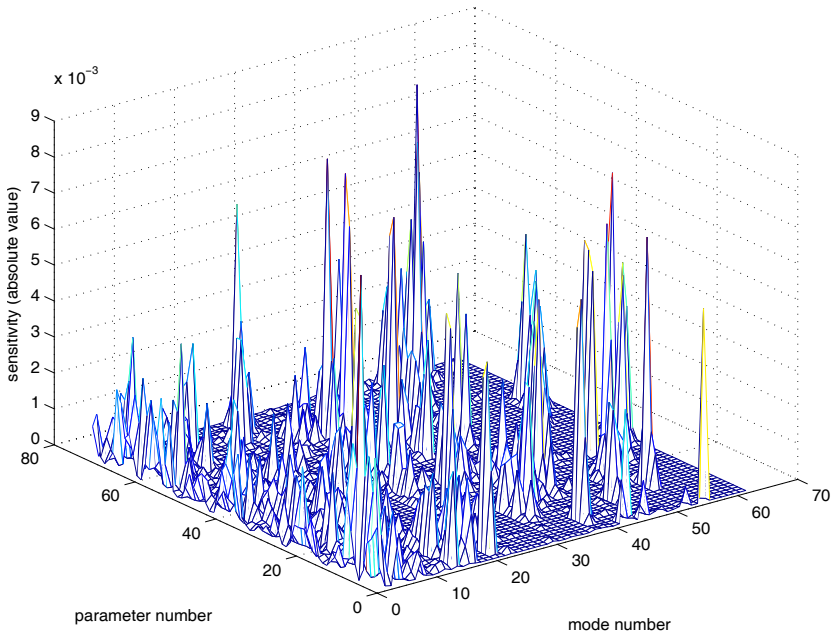

Figure 19: sensitivity to eigenfrequencies

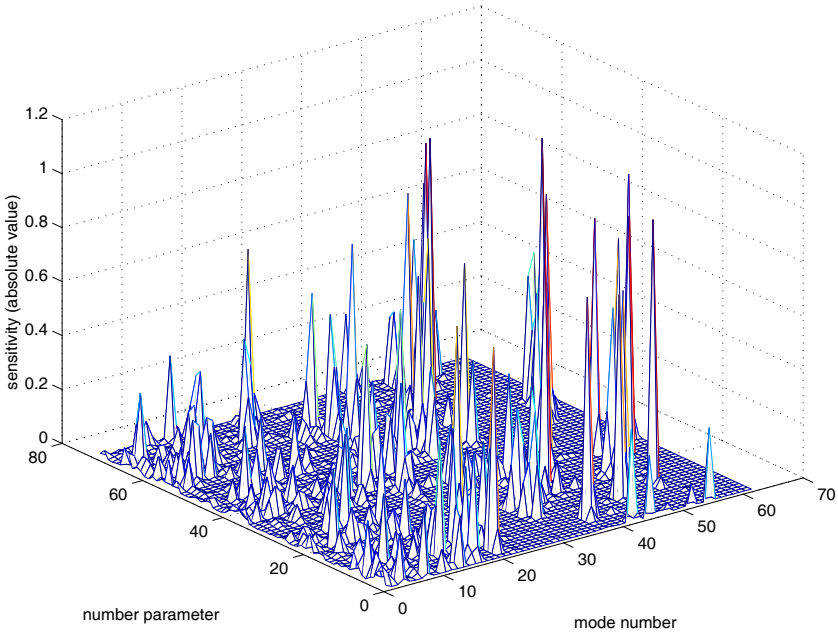

Figure 20: sensitivity to eigenvectors